

Interpebble contact radius in a comet nucleus

Sota Arakawa,^{1*} Daisuke Nishiura,¹ and Mikito Furuichi¹

¹*Japan Agency for Marine–Earth Science and Technology, 3173-25, Showa-machi, Kanazawa-ku, Yokohama, 236-0001, Japan*

Accepted 2023 March 21. Received 2023 March 08; in original form 2023 January 27

ABSTRACT

In recent years, the gravitational collapse of pebble clumps in the early Solar System has been regarded as a plausible scenario for the origin of comets. In this context, “pebbles” represent mm- to cm-sized dust aggregates composed of (sub)micron-sized dust particles, and the structure of km-sized comets is thought to be an agglomerate of pebbles. The contact radius for pebble–pebble contacts was modelled in an earlier study; however, the pressure dependence of the interpebble contact radius was not considered. Here, we revisit the interpebble contact radius in a comet nucleus. We calculated the interpebble contact radius based on JKR contact theory, and we took into consideration the effect of lithostatic pressure. We found that the interpebble contact radius varies with depth from the surface, and the earlier model underestimated it by one order of magnitude at the centre of the comet nucleus.

Key words: comets: general – planets and satellites: formation

1 INTRODUCTION

Comets are km-sized small bodies composed of volatile ices and refractory materials. They were formed in the outer region of the Solar System, where the temperature is sufficiently lower than the sublimation temperature of H₂O ice. Their origin and evolution provide important clues about the environment of the early Solar System.

In recent years, comet formation models advocating the gravitational collapse of pebble clumps have been intensively investigated (e.g., Blum et al. 2014, 2017; Johansen et al. 2014; Wahlberg Jansson & Johansen 2014; Lorek et al. 2016; Visser et al. 2021). In the context of comet formation, the word “pebbles” means mm- to cm-sized dust aggregates composed of (sub)micron-sized dust particles originating from the interstellar medium. In turbulent protoplanetary disks, micron-sized dust particles can grow into macroscopic pebbles via pairwise collisions (e.g., Blum & Wurm 2008; Arakawa et al. 2022a,b, 2023). Once the pebble radius reaches millimetres to centimetres, their collisional growth ends (e.g., Zsom et al. 2010; Lorek et al. 2018), and continued nonsticking collisions lead to rounding and compaction of pebbles (e.g., Weidling et al. 2009, 2012). In gaseous protoplanetary disks, pebbles can accumulate locally via aerodynamical processes (e.g., Johansen et al. 2014; Drazkowska et al. 2022), and km-sized comets are formed by the collapse of self-gravitating pebble clumps (e.g., Skorov & Blum 2012). The structure of km-sized comets formed via gravitational collapse of pebble clumps is deemed “hierarchical” aggregates, i.e., agglomerates of pebbles (e.g., Skorov & Blum 2012; Arakawa & Ohno 2020).

The physical properties of pebble-pile comets have been studied extensively by using laboratory experiments (e.g., Krause et al. 2011; Blum et al. 2014; Schräpler et al. 2015; Whizin et al. 2017; Katsuragi & Blum 2018; Malamud et al. 2022). Krause et al. (2011) measured the thermal conductivity of hierarchical aggregates under

high-vacuum conditions, and Gundlach & Blum (2012) developed a theoretical model that can reproduce the experimental results of Krause et al. (2011). Gundlach & Blum (2012) introduced the effective surface energy of pebbles for evaluation of the interpebble contact radius, which controls heat transfer through interpebble contacts (see also Weidling et al. 2012). Blum et al. (2014) studied the tensile strength of hierarchical aggregates of mm-sized pebbles. They revealed that the tensile strength of hierarchical aggregates increases with the compression pressure before breaking up. Irie et al. (2021) reported the cohesion strength between two pebbles in contact using the free-surface deformation of centrifuged hierarchical aggregates. The cohesion strength between two pebbles increases with the interpebble contact area (e.g., Arakawa 2020). Schräpler et al. (2015) investigated the compression curves of hierarchical aggregates, and they found that the filling factor is approximately constant when the compression pressure is lower than 10⁴ Pa (see also Heinisch et al. 2019; Malamud et al. 2022). The compression behaviour of hierarchical aggregates was investigated by several studies (e.g., Machii et al. 2013; Pacheco-Vázquez et al. 2021).

A theoretical model of the thermal conductivity of hierarchical aggregates was developed by Gundlach & Blum (2012). This model is widely used in the thermophysical modelling of pebble-pile comets (e.g., Capria et al. 2017; Skorov et al. 2017; Hu et al. 2019; Gundlach et al. 2020; Bischoff et al. 2021; Malamud et al. 2022). In the model of Gundlach & Blum (2012), the interpebble contact is modelled based on a contact theory for elastic spheres with surface energy, which is called JKR contact theory (Johnson et al. 1971). Then the interpebble contact radius is a function of the effective surface energy, the elastic properties of pebbles, and the pebble radius. We note, however, that the pressure dependence of the interpebble contact radius was not considered in Gundlach & Blum (2012) and their followers. If the interpebble contact radius strongly depends on the depth from the surface, we can imagine that both the thermal and mechanical properties of the comet nucleus also vary with depth.

* E-mail: arakawas@jamstec.go.jp (SA)

In this study, we revisit the interpebble contact radius in a comet nucleus. We calculate the interpebble contact radius based on JKR contact theory, and we take into consideration the effect of lithostatic pressure. We found that the interpebble contact radius should vary with depth from the surface. When the effective surface energy of pebbles is equal to that of Gundlach & Blum (2012), the effect of lithostatic pressure becomes important for the subsurface region where the depth is larger than $10\text{--}10^2$ cm, depending on the pebble radius. In Section 2, we review theoretical models that describe the particle–particle and pebble–pebble contacts. In Section 3, we present the results of some example calculations for a km-sized pebble-pile comet. We briefly discuss some uncertainties and caveats for the physical properties of pebbles and pebble piles in Section 4. A summary is presented in Section 5.

2 MODEL

2.1 JKR contact theory (Johnson et al. 1971)

In this section, we review JKR contact theory for elastic spheres with surface energy and external force (Johnson et al. 1971). Here, we consider the case in which two spheres in contact are made of the same material and have the same radius, r . Johnson et al. (1971) found that the contact radius, r_c , is given by

$$\begin{aligned} \frac{r_c}{r} &= \left[\frac{3(1-\nu^2)}{4Er^2} \left\{ F + \frac{3\pi}{2}\gamma r + \sqrt{3\pi\gamma r F + \left(\frac{3\pi}{2}\gamma r\right)^2} \right\} \right]^{1/3}, \\ &= \left[\frac{9\pi\gamma(1-\nu^2)}{4Er} \cdot \frac{1+2x+\sqrt{1+2x}}{2} \right]^{1/3}, \end{aligned} \quad (1)$$

where E is the Young’s modulus, ν is the Poisson’s ratio, and F is the external force acting on a sphere. Here, γ denotes the surface energy per unit contact area (i.e., the two surfaces in contact). We introduce a dimensionless parameter, x , that describes the strength of the external force:

$$x \equiv \frac{F}{3\pi\gamma r}. \quad (2)$$

When $x \ll 1$, r_c/r becomes

$$\frac{r_c}{r} \simeq \left[\frac{9\pi\gamma(1-\nu^2)}{4Er} \right]^{1/3}. \quad (3)$$

In contrast, when $x \gg 1$, r_c/r becomes

$$\frac{r_c}{r} \simeq \left[\frac{3(1-\nu^2)F}{4Er^2} \right]^{1/3}, \quad (4)$$

and the result is identical to that for Hertzian contact theory (Hertz 1896). It should be noted that both JKR and Hertzian contact theories are applicable for $r_c/r \ll 1$.

2.2 Contact between cohesive elastic pebbles

We also review the contact model for two pebbles in contact introduced by Weidling et al. (2012) and Gundlach & Blum (2012). They assumed that pebbles can be regarded as macroscopic elastic spheres

with effective surface energy. If there are no external forces acting on pebbles, the interpebble contact radius, $r_{c,\text{peb}}$, is given by

$$\frac{r_{c,\text{peb}}}{r_{\text{peb}}} = \left[\frac{9\pi\gamma_{\text{peb}}(1-\nu_{\text{peb}}^2)}{4E_{\text{peb}}r_{\text{peb}}} \right]^{1/3}, \quad (5)$$

where r_{peb} is the pebble radius, E_{peb} is the effective Young’s modulus of pebbles, ν_{peb} is the effective Poisson’s ratio of pebbles, and γ_{peb} is the effective surface energy of pebbles.

The effective surface energy of pebbles, γ_{peb} , is a key parameter that controls interpebble contacts. Gundlach & Blum (2012) proposed that γ_{peb} is given by the following equation (see also Weidling et al. 2012)¹:

$$\begin{aligned} \gamma_{\text{peb}} &= \phi_{\text{peb}}\gamma_{\text{par}} \left[\frac{9\pi(1-\nu_{\text{peb}}^2)}{r_{\text{par}}E_{\text{par}}} \right]^{2/3} \\ &= 5.4 \times 10^{-2} \text{ mJ m}^{-2}, \end{aligned} \quad (6)$$

where ϕ_{peb} denotes the filling factor inside pebbles, γ_{par} is the surface energy of particles, r_{par} is the particle radius, and E_{par} is the Young’s modulus of particles. The physical parameters used in this study are listed in Table 1 and are identical to those assumed in Gundlach et al. (2020) and Malamud et al. (2022).

The effective Young’s modulus of pebbles, E_{peb} , is also an important parameter that controls interpebble contacts. Based on the investigation by Weidling et al. (2012), many studies on pebble-pile comets (e.g., Blum et al. 2017; Hu et al. 2019; Gundlach et al. 2020; Bischoff et al. 2021; Malamud et al. 2022) assumed the following value for E_{peb} :

$$E_{\text{peb}} = 8.1 \text{ kPa}. \quad (7)$$

We note that E_{peb} must depend on the physical properties of pebbles and constituent particles (e.g., ϕ_{peb} , r_{par} , and γ_{par}) in reality (see Section 4.2.2).

When external forces act on pebbles, $r_{c,\text{peb}}$ should deviate from that predicted by Equation (5). Here we assumed that the dependence of $r_{c,\text{peb}}$ on the external force acting on pebbles, F_{peb} , is identical to that of Equation (1):

$$\frac{r_{c,\text{peb}}}{r_{\text{peb}}} = \left[\frac{9\pi\gamma_{\text{peb}}(1-\nu_{\text{peb}}^2)}{4E_{\text{peb}}r_{\text{peb}}} \cdot \frac{1+2x_{\text{peb}}+\sqrt{1+2x_{\text{peb}}}}{2} \right]^{1/3}, \quad (8)$$

where

$$x_{\text{peb}} = \frac{F_{\text{peb}}}{3\pi\gamma_{\text{peb}}r_{\text{peb}}}. \quad (9)$$

2.3 Interpebble force

When a pebble-pile layer is made of equal-sized spherical pebbles, the external force acting on a pebble, F_{peb} , should be proportional to the compressive stress, σ , as follows (see Sakatani et al. 2017):

$$F_{\text{peb}} = \frac{2\pi r_{\text{peb}}^2}{\sqrt{6}\phi_{\text{pack}}} \sigma, \quad (10)$$

¹ In the original derivation by Weidling et al. (2012), the Poisson’s ratio of particles, ν_{par} , was used instead of ν_{peb} in the calculation of γ_{peb} (Equation (6)). We note, however, that $\nu_{\text{par}} = \nu_{\text{peb}} = 0.17$ is assumed and the choice of Poisson’s ratio does not make any differences.

Table 1. List of physical parameters (see also Gundlach et al. 2020).

Parameter	Symbol	Value	Reference
Particle radius	r_{par}	1 μm	Gundlach et al. (2020)
Pebble radius	r_{peb}	1 mm or 1 cm	Malamud et al. (2022)
Surface energy of particles	γ_{par}	100 mJ m^{-2}	Gundlach et al. (2020)
Surface energy of pebbles	γ_{peb}	(see Equation (6))	Gundlach & Blum (2012)
Young's modulus of particles	E_{par}	55 GPa	Chan & Tien (1973)
Young's modulus of pebbles	E_{peb}	8.1 kPa	Weidling et al. (2012)
Poisson's ratio of particles	ν_{par}	0.17	Chan & Tien (1973)
Poisson's ratio of pebbles	ν_{peb}	0.17	Weidling et al. (2012)
Filling factor inside pebbles	ϕ_{peb}	0.4	Weidling et al. (2009)
Filling factor of pebble packing	ϕ_{pack}	0.6	Blum et al. (2014)
Bulk density of the comet nucleus	ρ_{comet}	532 kg m^{-3}	Jorda et al. (2016)
Material thermal conductivity	k_{mat}	(see Equations (A8) and (A9))	Malamud et al. (2022)
Rosseland mean opacity of particles	κ_{R}	(see Equation (A12))	Nakamoto & Nakagawa (1994)

where ϕ_{pack} is the filling factor of pebble packing.

In this study, we assume that the compressive stress inside the comet nucleus is caused by the lithostatic pressure. The lithostatic pressure inside a homogeneous object, σ , is given as a function of the depth d as follows (see Blum et al. 2017):

$$\sigma = \frac{2\pi}{3} \rho_{\text{comet}}^2 \mathcal{G} \left[R_{\text{comet}}^2 - (R_{\text{comet}} - d)^2 \right], \quad (11)$$

where \mathcal{G} is the gravitational constant, ρ_{comet} is the bulk density of the comet nucleus, and R_{comet} is the radius of the comet nucleus. The pressure at the centre, σ_{centre} , is given by

$$\sigma_{\text{centre}} = 40 \left(\frac{R_{\text{comet}}}{1 \text{ km}} \right)^2 \text{ Pa}. \quad (12)$$

When $d \ll R_{\text{comet}}$, σ is approximately given by

$$\begin{aligned} \sigma &\approx \frac{4\pi}{3} \rho_{\text{comet}}^2 \mathcal{G} R_{\text{comet}} d, \\ &\approx 7.9 \times 10^{-2} \left(\frac{R_{\text{comet}}}{1 \text{ km}} \right) \left(\frac{d}{1 \text{ m}} \right) \text{ Pa}, \end{aligned} \quad (13)$$

and σ is proportional to both R_{comet} and d .

It is usually assumed that both ϕ_{peb} and ϕ_{pack} are approximately constant in a nucleus of a km-sized pebble-pile comet (e.g., Blum et al. 2017, 2022). Here we briefly check the validity of this assumption. When pebbles have similar radii, Blum et al. (2017) noted that ϕ_{pack} would fall between random loose and close packing values (≈ 0.56 and ≈ 0.64 , respectively). Then ϕ_{pack} could be nearly constant unless pebbles deform by compression, and ϕ_{peb} barely changes when pebbles behave as elastic spheres. As discussed in Section 4.2.3, pebbles could indeed behave as elastic spheres and they may avoid significant deformation in the nucleus of a km-sized comet.

3 RESULTS

In this section, we present the results of some example calculations for a km-sized pebble-pile comet. We set $R_{\text{comet}} = 1 \text{ km}$ in this study. The interpebble contact radius and its dependence on depth are shown in Section 3.1, and the thermal conductivity in the comet nucleus is discussed in Section 3.2.

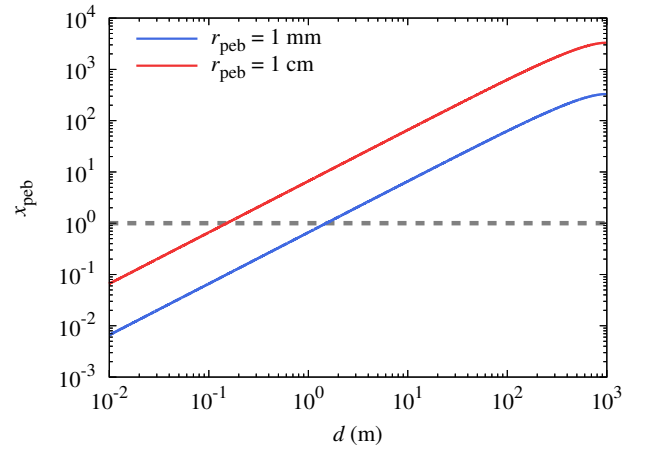


Figure 1. Dependence of x_{peb} on the depth from the surface, d . The grey dashed line represents $x_{\text{peb}} = 1$.

3.1 Interpebble contact radius

Figure 1 shows the dependence of x_{peb} on d . From Equations (9) and (10), the dependence of x_{peb} on σ and r_{peb} is given as follows:

$$x_{\text{peb}} = 84 \left(\frac{\sigma}{1 \text{ Pa}} \right) \left(\frac{r_{\text{peb}}}{1 \text{ cm}} \right). \quad (14)$$

At the centre of the comet nucleus, x_{peb} is orders of magnitude larger than 1. In contrast, we assume that σ is given by the lithostatic pressure and $x_{\text{peb}} = 0$ at the surface of the comet nucleus.

For $x_{\text{peb}} \ll 1$, the interpebble contact radius is given by Equation (5), and $r_{\text{c,peb}}/r_{\text{peb}}$ is proportional to $r_{\text{peb}}^{-1/3}$. In contrast, for $x_{\text{peb}} \gg 1$, the interpebble contact radius becomes

$$\frac{r_{\text{c,peb}}}{r_{\text{peb}}} \approx \left[\frac{\sqrt{6}\pi (1 - \nu_{\text{peb}}^2)}{4\phi_{\text{pack}} E_{\text{peb}}} \sigma \right]^{1/3}, \quad (15)$$

and we found that $r_{\text{c,peb}}/r_{\text{peb}}$ is nearly independent of r_{peb} . Figure 2 shows the dependence of $r_{\text{c,peb}}/r_{\text{peb}}$ on d . As predicted in Equation (15), $r_{\text{c,peb}}/r_{\text{peb}}$ is nearly independent of r_{peb} in the deep interior of the comet, where $x_{\text{peb}} \gg 1$. In contrast, $r_{\text{c,peb}}/r_{\text{peb}}$ clearly depends on r_{peb} but is independent of d in the shallow region.

When $x_{\text{peb}} \gg 1$, $r_{\text{c,peb}}/r_{\text{peb}}$ is given by Equation (15), and it is

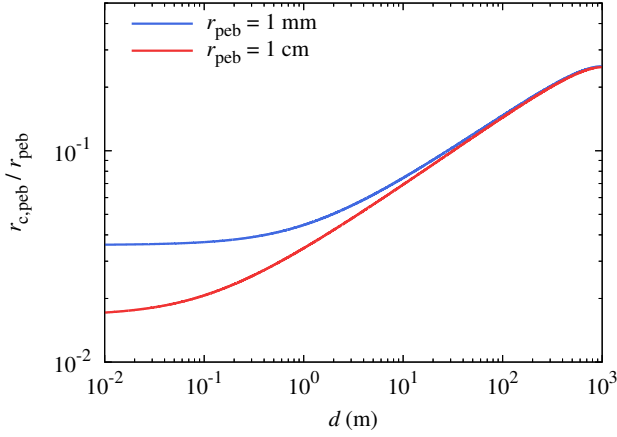


Figure 2. Dependence of $r_{c,peb}/r_{peb}$ on the depth from the surface, d .

approximated as

$$\frac{r_{c,peb}}{r_{peb}} \sim \left(\frac{\sigma}{E_{peb}} \right)^{1/3}. \quad (16)$$

As σ_{centre} is two orders of magnitude lower than E_{peb} , $r_{c,peb}/r_{peb} \ll 1$ is satisfied in the entire comet nucleus. Thus the JKR contact theory (Equation (8)) could be applicable for interpebble contacts in comet nuclei if pebbles behave as elastic spheres.

In Figure 1, we see that $x_{peb} < 1$ in the subsurface region of $d \lesssim 1$ m for $r_{peb} = 1$ mm. Even for $r_{peb} = 1$ cm, the subsurface region of $d \lesssim 10$ cm satisfies $x_{peb} < 1$. For comet 67P/Churyumov–Gerasimenko, which is the target of the *Rosetta* mission, the diurnal and seasonal thermal skin depths are evaluated as $\delta_{diurnal} \sim 1$ cm and $\delta_{seasonal} \sim 1$ m, respectively (e.g., Arakawa & Ohno 2020; Choukroun et al. 2020). Our results indicate that the diurnal variation in the subsurface temperature reflects the thermophysical properties of the uncompressed layer where $x_{peb} < 1$, while the seasonal variation might reflect the thermophysical properties of the compressed region where $x_{peb} \gtrsim 1$.

3.2 Thermal conductivity

The increase in $r_{c,peb}/r_{peb}$ in the comet nucleus could have large impacts on the physical properties. Here, we discuss the impacts of the increase in $r_{c,peb}/r_{peb}$ on the thermal conductivity. The thermal conductivity of a pebble-pile comet, k_{comet} , is given by the sum of two terms (e.g., Gundlach & Blum 2012; Gundlach et al. 2020):

$$k_{comet} = k_{net} + k_{rad}, \quad (17)$$

where k_{net} is the thermal conductivity through the solid particle contacts (i.e., network conduction; see Appendix A) and k_{rad} is the thermal conductivity due to radiation through the void space between the pebbles (see Appendix B). We note that k_{net} is proportional to $r_{c,peb}/r_{peb}$, while k_{rad} is independent of $r_{c,peb}/r_{peb}$. Therefore, k_{comet} significantly depends on d when $k_{net} \gg k_{rad}$, while k_{comet} is nearly independent of d when $k_{net} \ll k_{rad}$.

Figure 3 shows the dependence of k_{comet} on d , and Figure 4 shows k_{net}/k_{rad} as a function of d . In this study, we assume that the material thermal conductivity of constituent particles, k_{mat} , is set to be equal to that of H₂O ice for simplicity. It is known that the k_{mat} of ice particles strongly depends on whether they are crystalline or amorphous. The dependence of k_{mat} on T is given by Equation

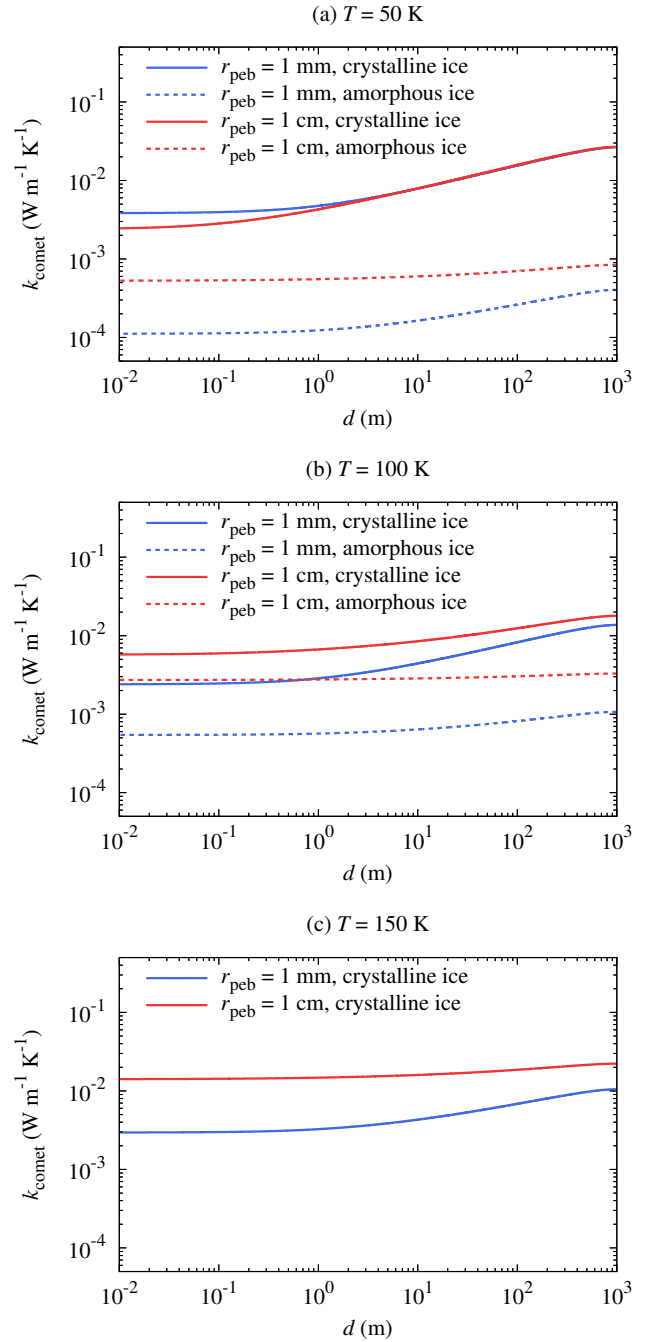


Figure 3. Dependence of k_{comet} on the depth from the surface, d . (a) For $T = 50$ K. (b) For $T = 100$ K. (c) For $T = 150$ K.

(A8) for crystalline ice and Equation (A9) for amorphous ice. We also assume that the temperature is homogeneous within the comet nucleus for simplicity.

We found that k_{comet} at $T = 50$ K is strongly dependent on d when pebbles are made of crystalline ice (Figure 3(a)); k_{comet} at the centre is approximately an order of magnitude higher than k_{comet} at the surface. Figure 4(a) shows that $k_{net} \gg k_{rad}$ is satisfied for this case. Therefore, k_{comet} is approximately proportional to $r_{c,peb}/r_{peb}$ and increases with d , as shown in Figure 2. In contrast, k_{comet} at $T = 50$ K barely depends on d when the pebble radius is $r_{peb} = 1$ cm

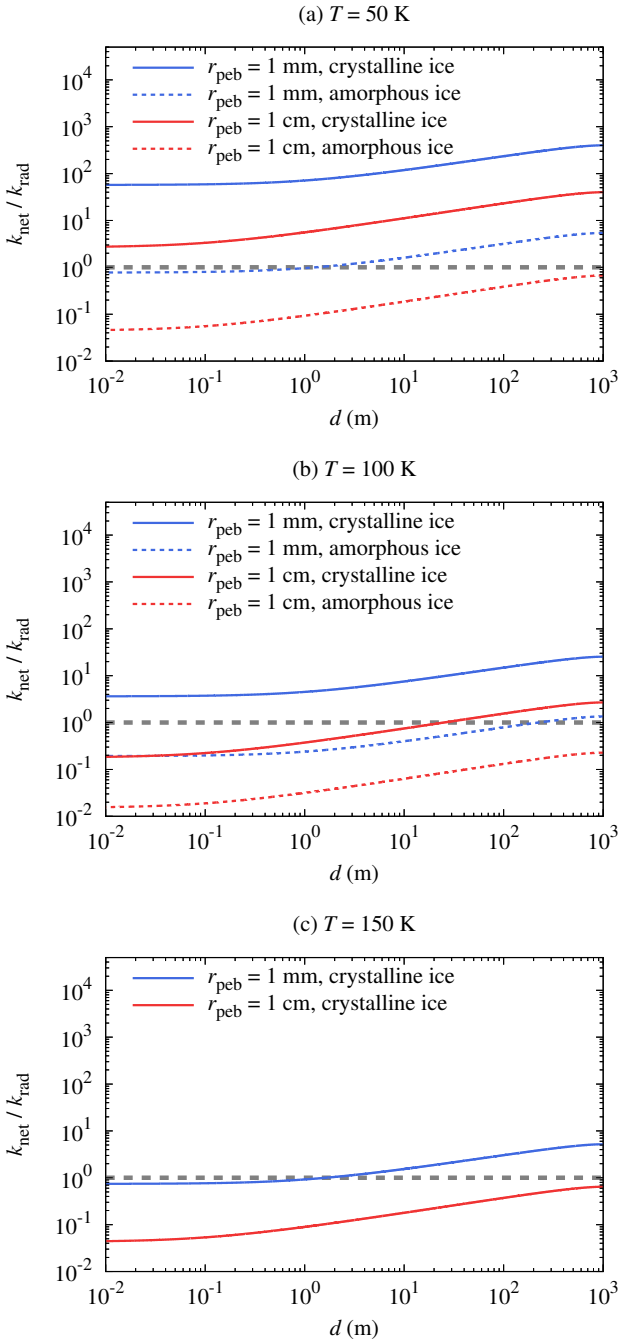


Figure 4. Dependence of $k_{\text{net}}/k_{\text{rad}}$ on the depth from the surface, d . (a) For $T = 50$ K. (b) For $T = 100$ K. (c) For $T = 150$ K. The grey dashed line represents $k_{\text{net}}/k_{\text{rad}} = 1$.

and they are made of amorphous ice. This is reasonable because $k_{\text{net}}/k_{\text{rad}} \ll 1$ in this case and k_{rad} is independent of d .

The dependence of k_{comet} on d at higher temperatures is shown in Figures 3(b) and 3(c). For a fixed pebble radius and state of ice, $k_{\text{net}}/k_{\text{rad}}$ decreases with increasing T (see Figure 4). At $T = 150$ K, k_{comet} barely depends on d when the pebble radius is $r_{\text{peb}} = 1$ cm and they are made of crystalline ice. We note that amorphous ice particles will crystallize at approximately $T \sim 100$ K (e.g., Kouchi et al.

2021; Malamud et al. 2022), and only crystalline ice is considered at $T = 150$ K.

The early thermal evolution of comets, during and immediately after formation, is the result of heating by radioactive decay of ^{26}Al and cooling by heat transfer from the hot comet nucleus to the cold space (e.g., Prialnik et al. 2008; Sirono 2017; Malamud et al. 2022). The cooling rate is proportional to the thermal conductivity, and the heating rate is proportional to the abundance of ^{26}Al , which decreases exponentially with time. The increase in k_{comet} in the comet nucleus should have impacts on the heating and cooling history of comets.

4 DISCUSSION

4.1 Possible impacts of an increase in the interpebble contact radius on the strength of the comet nucleus

In Section 3.2, we discuss the impact of an increase in the interpebble contact radius on the thermal conductivity. However, not only the thermal properties but also the strengths of pebble piles should depend on the interpebble contact radius. Here we briefly discuss possible impacts on the strength of the comet nucleus.

We revealed that the interpebble contact radius increases with depth, and $r_{c,\text{peb}}/r_{\text{peb}}$ at the centre of comets could be an order of magnitude larger than that at the surface (Figure 2). The interpebble contact area also increases with depth by two orders of magnitude. This may cause an increase in cohesion between pebbles, and the tensile and shear strengths of pebble piles might be depth-dependent. Indeed, laboratory experiments by Blum et al. (2014) reported that the tensile strength of pebble piles increases with the compression pressure before breaking up. We will discuss the possible impacts of depth-dependent strengths on the geological evolution of pebble-pile comets in future studies.

4.2 Model caveats

In this study, we calculated the interpebble contact radius and its dependence on depth using the material properties of pebbles (e.g., γ_{peb} and E_{peb}) derived by earlier studies (Gundlach & Blum 2012; Weidling et al. 2012). These parameters for pebbles are significantly different from those for constituent particles (see Table 1), and our results shown in Section 3 strongly depend on both γ_{peb} and E_{peb} . Here we discuss some uncertainties and caveats for these physical properties of pebbles.

4.2.1 Effective surface energy of pebbles

Although the canonical model of the effective surface energy of pebbles (Equation (6)), which is derived by Gundlach & Blum (2012), is widely used in earlier studies, a potential problem was noted by Arakawa (2020). Brisset et al. (2016) investigated the critical pull-off force for separating two sticking pebbles, F_{po} , and they found that $F_{\text{po}} \sim 10^{-7}$ N when the pebble radius is $r_{\text{peb}} \sim 0.1$ mm and constituent particles are micron-sized SiO_2 spheres. Arakawa (2020) revealed that the value of F_{po} obtained from laboratory experiments (Brisset et al. 2016) is an order of magnitude larger than that calculated from the effective surface energy modelled by Gundlach & Blum (2012). In other words, Equation (6) might underestimate the value of γ_{peb} when we discuss the critical pull-off force for separating two sticking pebbles.

For $x_{\text{peb}} \gg 1$, $r_{c,\text{peb}}/r_{\text{peb}}$ is nearly independent of γ_{peb} (Equation (15)). In contrast, $r_{c,\text{peb}}/r_{\text{peb}}$ increases with γ_{peb} when $x_{\text{peb}} \ll 1$,

$r_{c,peb}/r_{peb}$ (Equation (5)). Therefore, the thermal and physical properties of pebble piles in the shallow region ($d \ll 1$ m) would be strongly affected by the effective surface energy of pebbles, while the thermal evolution of the comet nucleus may not be sensitive to γ_{peb} .

We note that γ_{peb} must depend on the surface composition of the constituent particles. In earlier studies on the thermophysical modelling of comets (e.g., Gundlach et al. 2020; Malamud et al. 2022), a constant value of $\gamma_{par} = 100$ mJ m⁻² is assumed not only for pebbles composed of refractory particles but also for pebbles composed of icy particles. As Equation (6) predicted that γ_{peb} is proportional to $\gamma_{par}^{5/3}$, the dependence of γ_{peb} on the surface composition of constituent particles would be of great importance.

The composition of ice in the outer Solar System has been extensively studied (e.g., Altwegg et al. 2019; Krijt et al. 2020; Öberg & Bergin 2021). Except for H₂O, CO and CO₂ are thought to be the most prominent species in the outer Solar System, and laboratory experiments of collisions between CO₂ ice aggregates composed of micron-sized particles were performed by Fritscher & Teiser (2021). It is known that the material properties (γ_{par} , E_{par} , and ν_{par}) of CO₂ ice are close to those of H₂O ice (e.g., Arakawa & Krijt 2021; Fritscher & Teiser 2022), while the material properties of CO ice are poorly understood. The properties of icy particles may also depend on whether refractory materials are mantled by the icy layer (see Figure 1 of Arakawa & Ohno 2020) or whether refractory and icy materials are mixed well within each particle. Future studies on these points are essential to develop the physical modelling of pebble-pile comets.

4.2.2 Effective Young's modulus of pebbles

The canonical value of the effective Young's modulus of pebbles ($E_{peb} = 8.1$ kPa; see Equation (7)) is also widely used in earlier studies on pebble-pile comets. Weidling et al. (2012) performed microgravity experiments of free collisions between pebbles, and they found that the sticking velocity is $v_{stick} = 2.1 \times 10^{-4}$ m s⁻¹ for $r_{peb} = 0.5$ mm. Based on JKR contact theory, Weidling et al. (2012) derived the following equation for v_{stick} (see also Thornton & Ning 1998):

$$v_{stick} = 4.2 \left(\frac{\gamma_{peb}^5 r_{peb}^4}{m_{peb}^3 E_{peb}^2} \right)^{1/6}, \quad (18)$$

where $m_{peb} = (4\pi/3)\rho_{peb}r_{peb}^3$ is the pebble mass, and ρ_{peb} is the density of pebbles. Then Weidling et al. (2012) reported the value of $E_{peb} = 8.1$ kPa for pebbles whose filling factor is $\phi_{peb} = 0.35$ and constituent particles are micron-sized SiO₂ spheres.

We can imagine that E_{peb} must depend on many parameters including the filling factor of pebbles and the composition and radius of constituent particles, as is the case for γ_{peb} . Schröppler et al. (2022) investigated the collisional properties of cm-sized porous dust aggregates whose filling factor is approximately 10%. Then, they developed a method to calculate the dependence of E_{peb} (and ν_{peb}) on ϕ_{peb} . Their model indicates that $E_{peb} \sim 40$ – 60 kPa for icy pebbles when $\phi_{peb} \sim 0.1$ – 0.2 and $r_{par} \sim 3$ μ m, and $E_{peb} > 60$ kPa for $\phi_{peb} > 0.2$. The model also predicts that E_{peb} increases with decreasing r_{par} . The typical particle radius in the interstellar medium is $r_{par} \sim 0.1$ μ m (e.g., Mathis et al. 1977). Tazaki & Dominik (2022) revealed that the results of optical and near-infrared polarimetric observations are consistent with dust aggregates in extrasolar protoplanetary disks that are also composed of submicron-sized particles. Thus, the value of E_{peb} for *natural* pebble piles (i.e., comets in the

Solar System) might be orders of magnitude higher than that assumed in this study ($E_{peb} = 8.1$ kPa). We will discuss this point in the future by numerical simulations using the discrete element method (e.g., Furuichi et al. 2018).

It is important to note that $r_{c,peb}/r_{peb}$ is proportional to $E_{peb}^{-1/3}$ for the cases of both $x_{peb} < 1$ and $x_{peb} > 1$ (Equation (8)). If the true value of E_{peb} is three orders of magnitude larger than the canonical value, the thermal conductivity through the solid particle contacts would be one order of magnitude smaller than shown in Section 3.2. In this case, k_{comet} for amorphous ice (dashed lines in Figure 3) is approximately given by $k_{comet} \simeq k_{rad}$ and is independent of d when the temperature and the pebble radius are constant over depth.

4.2.3 Plastic yielding of pebbles

In this study, we assume that pebbles behave as elastic spheres. However, it is evident that pebbles no longer behave as elastic spheres when F_{peb} exceeds the threshold for plastic yielding. Okubo & Katsuragi (2022) measured the peak compression force at the yielding point, F_{peak} , and they found that $F_{peak}/(\pi r_{peb}^2) = (18 \pm 7)$ kPa for dry pebbles of $r_{peb} = 1.5$ mm, $\phi_{peb} = 0.26$, and constituent particles are $r_{par} = 2.5$ μ m-sized glass beads. The value of $F_{peb}/(\pi r_{peb}^2)$ at the centre of a km-sized comet is roughly given by $\sigma_{centre} = 40(R_{comet}/1 \text{ km})^2$ Pa (see Equation (12)), which is orders of magnitude lower than $F_{peak}/(\pi r_{peb}^2)$. Thus, dry pebbles used in Okubo & Katsuragi (2022) might behave as elastic spheres in a comet nucleus.

The value of $F_{peak}/(\pi r_{peb}^2) = (18 \pm 7)$ kPa may also be consistent with the compression curves of hierarchical aggregates (e.g., Schröppler et al. 2015; Heinisch et al. 2019). They reported that the total filling factor of pebble piles is approximately constant when $\sigma < 10$ kPa. It is thought that compression of pebble piles starts when deformation and destruction of pebbles occurs (e.g., Blum et al. 2022). We note that F_{peak} must depend on many parameters, including ϕ_{peb} and r_{par} . In addition, F_{peak} increases significantly when pebbles are sintered (e.g., Okubo & Katsuragi 2022). As most related experiments are for pebbles composed of micron-sized glass beads, future studies on the onset of plastic yielding of icy pebbles are necessary.

5 CONCLUSIONS

The physical properties of pebble piles have been studied extensively by laboratory experiments. These studies highlighted the importance of pebble-pebble contacts for the physical modelling of pebble-pile comets. The contact radius for pebble-pebble contacts was modelled by Gundlach & Blum (2012); however, the pressure dependence of the interpebble contact radius was not considered in their model.

In this study, we revisited the interpebble contact radius in a comet nucleus (see Section 2). We calculated the interpebble contact radius based on JKR contact theory (Johnson et al. 1971), and we took into consideration the effect of lithostatic pressure. We found that the interpebble contact radius varies with depth from the surface, and the earlier model underestimated it by one order of magnitude at the centre of the comet nucleus (see Section 3.1).

We also evaluated the impact of the increase in the interpebble contact radius on the thermal conductivity of a pebble-pile comet (see Section 3.2). We found that when pebbles are cm-sized and made of crystalline ice, the thermal conductivity through interpebble contacts is larger than the thermal conductivity due to radiation through the void space between pebbles. In this case, the thermal conductivity of a pebble-pile comet is proportional to the interpebble contact radius,

which increases with depth. In contrast, when pebbles are mm-sized and made of amorphous ice, the thermal conductivity of a pebble-pile comet is nearly independent of the depth. The impacts of modification of the thermal conductivity on the early thermal evolution of comets will be discussed in our future studies.

We note that both the effective surface energy and Young's modulus of pebbles are still under debate (see Section 4.2). These parameters should depend on many physical parameters of pebbles and their constituent particles, and several prediction models have been proposed (e.g., Gundlach & Blum 2012; Schr apler et al. 2022). Recently, Schr apler et al. (2022) proposed a novel model to describe the filling factor dependence of the effective surface energy and Young's modulus of pebbles. Their proposed model was used for interpreting their experimental results on dynamic pebble–pebble collisions. Although their model was originally derived for the case of $\phi_{\text{peb}} < 0.33$, it might be worthwhile to investigate the quasistatic behavior of pebble piles on the basis of their model in future studies.

It is also a problem that the physical properties of pebbles composed of submicron-sized particles are barely investigated in laboratories, although comets in the Solar System would be made of pebbles composed of submicron-sized particles. As submicron-sized particles are usually used in numerical simulations, future collaborations between numerical simulations and laboratory experiments might be the key to unveiling the nature of pebble-pile comets.

ACKNOWLEDGEMENTS

The authors wish to express their cordial thanks to the referee J urgen Blum for constructive comments. This study was supported by a Grant-in-Aid for Scientific Research (JP18K03815) from the Japan Society for the Promotion of Science (JSPS). We thank American Journal Experts (AJE) for English language editing.

DATA AVAILABILITY

The data underlying this article will be shared on reasonable request to the corresponding author.

REFERENCES

- Altwegg K., Balsiger H., Fuselier S. A., 2019, *ARA&A*, 57, 113
 Arakawa S., 2020, *MNRAS*, 496, 2786
 Arakawa S., Krijt S., 2021, *ApJ*, 910, 130
 Arakawa S., Ohno K., 2020, *MNRAS*, 497, 1166
 Arakawa S., Tanaka H., Kataoka A., Nakamoto T., 2017, *A&A*, 608, L7
 Arakawa S., Tatsuuma M., Sakatani N., Nakamoto T., 2019a, *Icarus*, 324, 8
 Arakawa S., Takemoto M., Nakamoto T., 2019b, *Progress of Theoretical and Experimental Physics*, 2019, 093E02
 Arakawa S., Tanaka H., Kokubo E., 2022a, *ApJ*, 933, 144
 Arakawa S., Tanaka H., Kokubo E., 2022b, *ApJ*, 939, 100
 Arakawa S., Tanaka H., Kokubo E., Nishiura D., Furuichi M., 2023, *A&A*, 670, L21
 Bischoff D., Gundlach B., Blum J., 2021, *MNRAS*, 508, 4705
 Blum J., Wurm G., 2008, *ARA&A*, 46, 21
 Blum J., Gundlach B., M uhle S., Trigo-Rodr ıguez J. M., 2014, *Icarus*, 235, 156
 Blum J., et al., 2017, *MNRAS*, 469, S755
 Blum J., Bischoff D., Gundlach B., 2022, *Universe*, 8, 381
 Brisset J., Hei elmann D., Kothe S., Weidling R., Blum J., 2016, *A&A*, 593, A3
 Capria M. T., et al., 2017, *MNRAS*, 469, S685
 Chan C. K., Tien C. L., 1973, *Journal of Heat Transfer*, 95, 302

- Choukroun M., et al., 2020, *Space Sci. Rev.*, 216, 44
 Drazkowska J., et al., 2022, arXiv e-prints, p. arXiv:2203.09759
 Fritscher M., Teiser J., 2021, *ApJ*, 923, 134
 Fritscher M., Teiser J., 2022, *MNRAS*, 512, 3754
 Furuichi M., Nishiura D., Kuwano O., Bauville A., Hori T., Sakaguchi H., 2018, *Scientific Reports*, 8, 8685
 Gundlach B., Blum J., 2012, *Icarus*, 219, 618
 Gundlach B., Fulle M., Blum J., 2020, *MNRAS*, 493, 3690
 Heinisch P., et al., 2019, *A&A*, 630, A2
 Hertz H., 1896, *Miscellaneous papers*. Macmillan
 Hu X., Gundlach B., von Borstel I., Blum J., Shi X., 2019, *A&A*, 630, A5
 Irie T., Yamaguchi R., Watanabe S.-i., Katsuragi H., 2021, *Measurement Science and Technology*, 32, 125301
 Johansen A., Blum J., Tanaka H., Ormel C., Bizzarro M., Rickman H., 2014, in Beuther H., Klessen R. S., Dullemond C. P., Henning T., eds, *Protostars and Planets VI*. p. 547 (arXiv:1402.1344), doi:10.2458/azu_uapress_9780816531240-ch024
 Johnson K. L., Kendall K., Roberts A. D., 1971, *Proceedings of the Royal Society of London Series A*, 324, 301
 Jorda L., et al., 2016, *Icarus*, 277, 257
 Katsuragi H., Blum J., 2018, *Phys. Rev. Lett.*, 121, 208001
 Klinger J., 1980, *Science*, 209, 271
 Kouchi A., Greenberg J. M., Yamamoto T., Mukai T., 1992, *ApJ*, 388, L73
 Kouchi A., et al., 2021, *ApJ*, 918, 45
 Krause M., Blum J., Skorov Y. V., Trieloff M., 2011, *Icarus*, 214, 286
 Krijt S., Bosman A. D., Zhang K., Schwarz K. R., Ciesla F. J., Bergin E. A., 2020, *ApJ*, 899, 134
 Lorek S., Gundlach B., Lacerda P., Blum J., 2016, *A&A*, 587, A128
 Lorek S., Lacerda P., Blum J., 2018, *A&A*, 611, A18
 Machii N., Nakamura A. M., G uttler C., Beger D., Blum J., 2013, *Icarus*, 226, 111
 Malamud U., Landeck W. A., Bischoff D., Kreuzig C., Perets H. B., Gundlach B., Blum J., 2022, *MNRAS*, 514, 3366
 Mathis J. S., Rumpl W., Nordsieck K. H., 1977, *ApJ*, 217, 425
 Nakamoto T., Nakagawa Y., 1994, *ApJ*, 421, 640
  berg K. I., Bergin E. A., 2021, *Phys. Rep.*, 893, 1
 Okubo F., Katsuragi H., 2022, *A&A*, 664, A147
 Pacheco-V azquez F., Omura T., Katsuragi H., 2021, *Physical Review Research*, 3, 013190
 Prialnik D., Sarid G., Rosenberg E. D., Merk R., 2008, *Space Sci. Rev.*, 138, 147
 Ryan A. J., Pino Mu oz D., Bernacki M., Delbo M., 2020, *Journal of Geophysical Research (Planets)*, 125, e06100
 Ryan A. J., Pino Mu oz D., Bernacki M., Delbo M., Sakatani N., Biele J., Emery J. P., Rozitis B., 2022, *Journal of Geophysical Research (Planets)*, 127, e07191
 Sakatani N., Ogawa K., Iijima Y., Arakawa M., Honda R., Tanaka S., 2017, *AIP Advances*, 7, 015310
 Schr apler R., Blum J., von Borstel I., G uttler C., 2015, *Icarus*, 257, 33
 Schr apler R. R., Landeck W. A., Blum J., 2022, *MNRAS*, 509, 5641
 Sirono S.-i., 2017, *ApJ*, 842, 11
 Skorov Y., Blum J., 2012, *Icarus*, 221, 1
 Skorov Y. V., Rezac L., Hartogh P., Keller H. U., 2017, *A&A*, 600, A142
 Tazaki R., Dominik C., 2022, *A&A*, 663, A57
 Thornton C., Ning Z., 1998, *Powder Technology*, 99, 154
 Visser R. G., Drazkowska J., Dominik C., 2021, *A&A*, 647, A126
 Wahlberg Jansson K., Johansen A., 2014, *A&A*, 570, A47
 Weidling R., G uttler C., Blum J., Brauer F., 2009, *ApJ*, 696, 2036
 Weidling R., G uttler C., Blum J., 2012, *Icarus*, 218, 688
 Whizin A. D., Blum J., Colwell J. E., 2017, *ApJ*, 836, 94
 Zsom A., Ormel C. W., G uttler C., Blum J., Dullemond C. P., 2010, *A&A*, 513, A57

APPENDIX A: THERMAL CONDUCTIVITY THROUGH INTERPEBBLE CONTACTS

The thermal conductivity through particle contacts is modelled in our previous studies (Arakawa et al. 2017, 2019a,b). The thermal conductivity through interpebble contacts, k_{net} , is given by

$$k_{\text{net}} = 2k_{\text{peb}} \frac{r_{\text{c,peb}}}{r_{\text{peb}}} f(\phi_{\text{pack}}), \quad (\text{A1})$$

where f is a dimensionless function associated with packing geometry. Arakawa et al. (2019a) found that f is given as a function of the filling factor, ϕ :

$$f(\phi) = 0.784\phi^{1.99} \left(\frac{Z(\phi)}{2} \right)^{0.556}, \quad (\text{A2})$$

where Z denotes the average coordination number that also depends on ϕ (Arakawa et al. 2019a,b):

$$Z(\phi) = 2 + 9.38\phi^{1.62}. \quad (\text{A3})$$

The thermal conductivity within a pebble, k_{peb} , is given by the sum of two terms:

$$k_{\text{peb}} = k_{\text{net,peb}} + k_{\text{rad,peb}}, \quad (\text{A4})$$

where $k_{\text{net,peb}}$ is the thermal conductivity through contacts of constituent particles and $k_{\text{rad,peb}}$ is the thermal conductivity due to radiation within a pebble.

When the contact radius between constituent particles is $r_{\text{c,par}}$, $k_{\text{net,peb}}$ is given by

$$k_{\text{net,peb}} = 2k_{\text{mat}} \frac{r_{\text{c,par}}}{r_{\text{par}}} f(\phi_{\text{peb}}). \quad (\text{A5})$$

Here we note that $r_{\text{c,par}}$ in the comet nucleus is nearly independent of d . The external force acting on a particle, F_{par} , is roughly given by $F_{\text{par}} \sim \pi r_{\text{par}}^2 \sigma$ (e.g., Chan & Tien 1973; Sakatani et al. 2017). We evaluate the x parameter introduced in Equation (2). For contacts between constituent particles, we define x_{par} as follows:

$$\begin{aligned} x_{\text{par}} &= \frac{F_{\text{par}}}{3\pi\gamma_{\text{par}}r_{\text{par}}} \\ &\sim \frac{r_{\text{par}}\sigma}{\gamma_{\text{par}}} \\ &\sim 10^{-3} \left(\frac{\sigma}{10^2 \text{ Pa}} \right), \end{aligned} \quad (\text{A6})$$

and $x_{\text{par}} \ll 1$ in the entire comet nucleus. In this study, we assume that $r_{\text{c,par}}$ is given by

$$\frac{r_{\text{c,par}}}{r_{\text{par}}} = \left[\frac{9\pi\gamma_{\text{par}}(1 - \nu_{\text{par}}^2)}{4E_{\text{par}}r_{\text{par}}} \right]^{1/3}. \quad (\text{A7})$$

The material thermal conductivity of ice, k_{mat} , is set to be equal to that assumed in Malamud et al. (2022). It is known that k_{mat} depends on whether ice is crystalline or amorphous (e.g., Klinger 1980; Kouchi et al. 1992). For crystalline ice, k_{mat} is given by

$$k_{\text{mat}} = 5.67 \left(\frac{T}{100 \text{ K}} \right)^{-1} \text{ W m}^{-1} \text{ K}^{-1}, \quad (\text{A8})$$

while for amorphous ice, k_{mat} is given by

$$k_{\text{mat}} = \left[2.348 \times 10^{-1} \left(\frac{T}{100 \text{ K}} \right) + 2.82 \times 10^{-2} \right] \text{ W m}^{-1} \text{ K}^{-1}. \quad (\text{A9})$$

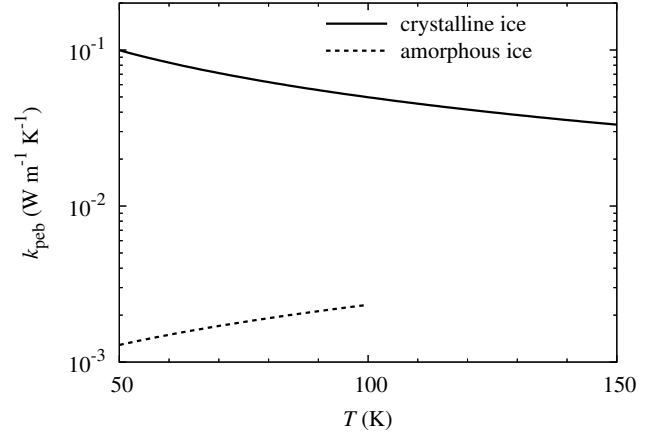


Figure A1. Thermal conductivity within a pebble, k_{peb} , as a function of temperature, T . We note that the temperature range of $T \leq 100$ K is considered for amorphous ice because it crystallizes at $T \approx 100$ K.

When constituent particles are optically thin, Arakawa et al. (2017) found that $k_{\text{rad,peb}}$ is given by

$$k_{\text{rad,peb}} = \frac{16}{3} \sigma_{\text{SB}} T^3 l_{\text{mfp}}, \quad (\text{A10})$$

where σ_{SB} is the Stefan–Boltzmann constant and l_{mfp} is the mean free path of photons. When the Rosseland mean opacity of particles is κ_{R} , l_{mfp} is given by

$$l_{\text{mfp}} = \frac{1}{\kappa_{\text{R}} \rho_{\text{peb}}}. \quad (\text{A11})$$

The density of pebbles, ρ_{peb} , is $\rho_{\text{peb}} = \rho_{\text{comet}} / \phi_{\text{pack}} = 887 \text{ kg m}^{-3}$.

The Rosseland mean opacity increases as $\kappa_{\text{R}} \propto T^2$ for $T < 150$ K (e.g., Nakamoto & Nakagawa 1994):

$$\kappa_{\text{R}} = 20 \left(\frac{T}{100 \text{ K}} \right)^2 \text{ m}^2 \text{ kg}^{-1}. \quad (\text{A12})$$

For the temperature range between 50 K and 150 K, we found the following relation:

$$r_{\text{par}} \ll l_{\text{mfp}} \ll r_{\text{peb}}, \quad (\text{A13})$$

is satisfied; in other words, mm- to cm-sized pebbles are optically thick but 1 μm -sized constituent particles are optically thin in the comet nucleus. These are consistent with the assumptions of our modelling.

We found that $k_{\text{rad,peb}} \sim 10^{-5} \text{ W m}^{-1} \text{ K}^{-1}$ is orders of magnitude lower than $k_{\text{net,peb}}$ and $k_{\text{peb}} \approx k_{\text{net,peb}}$ in our simulations (see Figure A1). We also note that the contribution of $k_{\text{rad,peb}}$ is ignored in earlier studies (e.g., Gundlach et al. 2020; Malamud et al. 2022).

APPENDIX B: THERMAL CONDUCTIVITY DUE TO RADIATION

Heat transfer due to radiation is of great importance for porous granular matter. When the thermal conductivity due to radiation is comparable to or lower than the thermal conductivity of the constituting spheres, the nonisothermality within a sphere affects the heat transfer (e.g., Ryan et al. 2020, 2022). We take into consideration this effect.

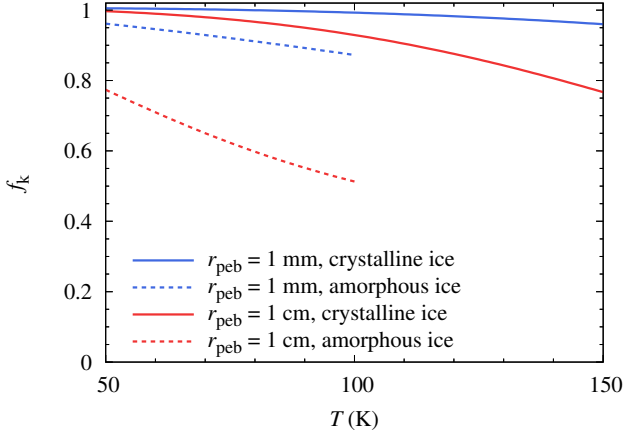


Figure B1. The nonisothermal correction factor, f_k , as a function of the temperature, T (see Equations (B1) and (B3)).

For a pebble pile, the thermal conductivity due to radiation through the void space between pebbles, k_{rad} , is given by

$$k_{\text{rad}} = 8\sigma_{\text{SB}}T^3 r_{\text{peb}} \mathcal{F}(\phi_{\text{pack}}) f_k(k_{\text{peb}}, r_{\text{peb}}, \phi_{\text{pack}}, T). \quad (\text{B1})$$

Based on numerical simulations, Ryan et al. (2022) found that the radiative exchange factor, \mathcal{F} , is given by

$$\mathcal{F}(\phi) = 0.739 + 0.629 \left(\frac{1-\phi}{\phi} \right)^{1.031}, \quad (\text{B2})$$

and the nonisothermal correction factor, f_k , is given by

$$f_k(k, r, \phi, T) = 1.007 - 0.500 \arctan \left[1.351 \left(\frac{8\sigma_{\text{SB}} r \phi T^3}{k} \right)^{0.741} \right]. \quad (\text{B3})$$

We note that Equation (B1) is applicable only when each pebble is optically thick (Ryan et al. 2022). We confirmed that mm- to cm-sized pebbles are indeed optically thick (see Relation (A13)).

Figure B1 shows $f_k(k_{\text{peb}}, r_{\text{peb}}, \phi_{\text{pack}}, T)$ as a function of T . We found that f_k for amorphous ice is lower than that for crystalline ice, and f_k decreases with increasing r_{peb} . We can understand these relations from Equation (B3). We note that the validity of Equation (B3) has not yet been confirmed for $f_k < 0.4$ (see Figure 4 of Ryan et al. 2022). Future studies on the nonisothermal effect would be needed when we discuss k_{rad} for pebble pile comets made of larger pebbles ($r_{\text{peb}} \gg 1$ cm) or higher temperature ($T \gg 150$ K).

This paper has been typeset from a $\text{\TeX}/\text{\LaTeX}$ file prepared by the author.